ELSEVIER

International Journal of Pressure Vessels and Piping 79 (2002) 297–308

INTERNATIONAL JOURNAL OF
Pressure Vessels and Piping

www.elsevier.com/locate/ijpvp

Strengthening of BWR Mark III reinforced concrete containment with fibre composite laminate material

H.-T. Hu*, T.-F. Chou

Department of Civil Engineering, National Cheng Kung University, Tainan 70101, Taiwan, ROC

Received 7 March 2001; revised 29 January 2002; accepted 29 January 2002

Abstract

Numerical analyses are carried out by using the ABAQUS finite element program to predict the ultimate pressure capacity and the failure mode of the BWR Mark III reinforced concrete containment strengthened by composite materials or steel plates at various positions. Material non-linear behaviour for concrete, steel, and fibre composite laminate material are all simulated with proper constitutive models. It has been shown that the use of $[\pm\theta/90/0]_{5S}$ composite materials with $50 \leq \theta \leq 90^{\circ}$ to strengthen the containment at the upper cylinder and the dome achieves the most satisfactory strengthening results. (The fibre angle of the lamina is measured counter-clockwise through the outward normal direction from the meridian of the containment shell structure.)

Keywords: Strengthen; Reinforced concrete containment; Composite laminate materials

1. Introduction

After the accident at the Three Mile Island nuclear plant in 1979, it has become necessary to perform failure analysis and calculate the ultimate pressure capability of the nuclear reactor containment for the safety assessment of nuclear power plants [1–3]. Since the 70s, non-linear material constitutive models and non-linear finite element solution techniques have been continuously and successfully developed [4–9], enabling the ultimate pressure capability of the nuclear reactor containment to be predicted more accurately [10–13].

One of the research projects [13], sponsored by the Atomic Energy Council, Taiwan, ROC, shows that the ultimate internal pressure capacity of the BWR Mark III reinforced concrete containment at Kuosheng nuclear power plant is 164.6 kPa. This ultimate internal pressure capacity is about 59.2% higher than the design load 103.4 kPa [14] and the containment structures are proved to be safe in service. These reinforced concrete containment structures were built in the late 70s and the design life cycle is 40 years. Due to the difficulty in finding a replacement energy source, extension of the life cycle for these nuclear power plants might be needed. It is known that the mechanical properties of the containment materials degrade with time. Consequently, after long-term service, the ultimate pressure strength of the containment would be lower than the initial design value and the strengthening of the containment structure may become necessary.

The traditional material used in strengthening of concrete structures is steel. Because of drawbacks of low corrosion resistance and handling problems involving excessive size and weight, there is a need to look for alternatives. Due to light weight, high strength, good fatigue, and corrosion properties, fibre composite laminate materials have been intensively used for repairing and strengthening of aerospace structures [15–18]. Although, the study of using composite laminate materials to strengthen reinforced concrete structures only started in the 90s [19–22], it is feasible to use the technology in the near future.

In this paper, the finite element program ABAQUS [23] is used to perform the ultimate analysis of the BWR Mark III reinforced concrete containment, strengthened by steel plates or fibre composite laminate materials, at Kuosheng nuclear power plant. The geometry and finite element mesh of the containment are reviewed first. Then, material properties of reinforcing steel, liner plate, strengthening steel plate, concrete, and laminate composite material are given and proper constitutive models are introduced to simulate their non-linear behaviours. Finally, failure analyses of the reinforced concrete containment strengthened by steel plates or laminate composite materials at various positions and subjected to internal pressure are carried out and important conclusions are given.

* Corresponding author. Tel.: +886-6-2757-575x63168; fax: +886-6-2358-542.

E-mail address: hthu@mail.ncku.edu.tw (H.-T. Hu).

0308-0161/02/$ - see front matter
PII: S0308-0161(02)00016-9

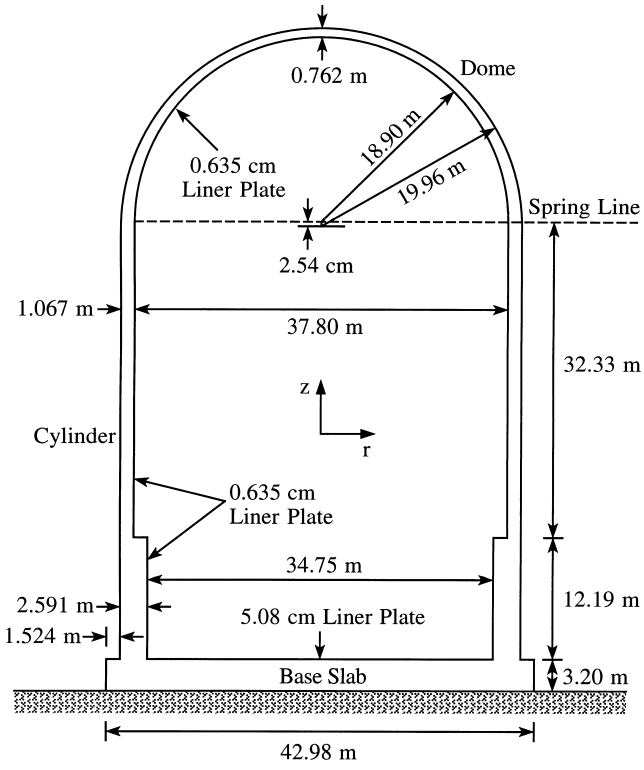

Fig. 1. Geometry and dimensions of the BWR reinforced concrete containment of Kuosheng nuclear power plant.

2. Containment geometry and finite element mesh

The BWR reinforced concrete containment at Kuosheng nuclear power plant is composed of a circular base slab, an upright cylinder, and a hemispherical dome (Fig. 1). To simplify the analysis, equipment hatches and penetrations on the containment are not considered and the structural geometry is assumed to be axisymmetric. The top of the containment is about 67.05 m above ground. The inner radius of the dome is 18.90 m. The thickness of the dome varies from 0.762 m at the apex to 1.067 m at the spring line. The inner diameters of the upper and lower cylinders are 37.80 and 34.75 m. The thicknesses of the upper and lower cylinders are 1.067 and 2.591 m, respectively. The base slab is made of a 3.2 m thick flat circular plate with a diameter of 42.98 m.

The entire interior surface of the dome, cylinder, and base slab are lined with a continuous steel plate system to provide a leak-tight barrier. The thickness of the steel liner plate inside the dome and cylinder is 0.635 cm while the thickness of the steel plate on the base slab is 5.08 cm. Most of the steel reinforcing bars are placed in an axisymmetric manner in the containment and the detailed arrangements of steel reinforcing bars are given in the Final Safety Analysis Report of the Kuosheng nuclear power plant [14]. Because some steel reinforcement layers in the base slab are placed in directions parallel to the x and y axes, the deformation of the containment will no longer be axisymmetric and will have four planes of symmetry (Fig. 2a). As a result, only 1/8 part of the structure is analysed and the boundary conditions imposed on the symmetry planes are displacements in the circumferential direction, rotations in the radial direction and rotations in the z direction to be zero. In the numerical simulation, 8-node shell elements (six degrees of freedom per node) are used to model the parts of the dome and cylinder, and 27-node solid elements (three degrees of freedom per node) are used to model the base slab (Fig. 2b). The liner plates are also modelled by 8-node shell elements. They are either linked to the shell elements of the concrete section (without any offset) at the parts of dome and cylinder, or attached to the inner surface of the solid elements at the base slab. The formulation of the 8-node shell allows transverse shear deformation and these shear flexible shell elements can be used for both thick and thin shell analysis [23]. At the bottom of the base slab, special purpose 9-node interface elements are used to link the base slab to the ground. The interface elements allow the contact surfaces between the base slab and the ground to remain closed or open but not to penetrate each other. When fibre composite laminate materials or steel plates are utilised to strengthen the containment, they are also modelled by 8-node shell elements, which are superimposed on the shell elements of the concrete section (without any offset).

3. Material properties and constitutive models

The materials used in the analysis involve steel reinforcing bar, steel liner plate, strengthening steel plate, concrete, and fibre composite laminate material. The constitutive models for steel reinforcing bar, steel liner plate,

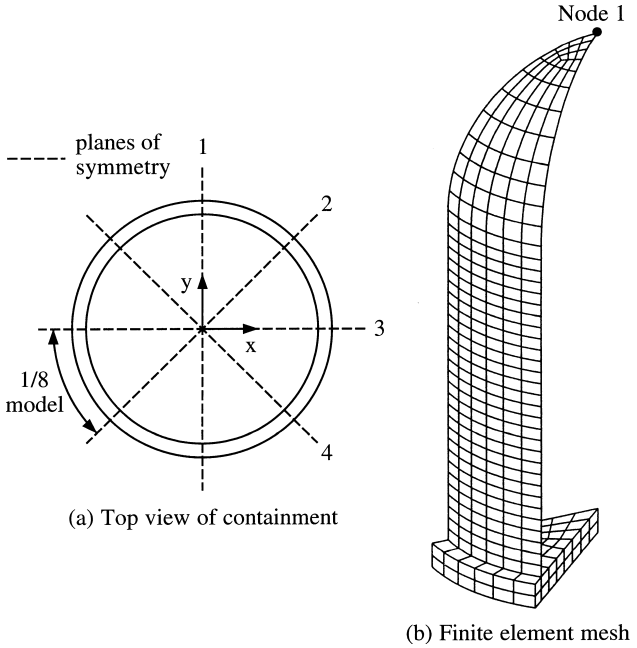

Fig. 2. 1/8 model of the BWR Mark III reinforced concrete containment of Kuosheng nuclear power plant.

strengthening steel plate, and concrete are available in the ABAQUS material library [23]. Thus, their input material properties and constitutive models are briefly discussed. The ABAQUS program does not have a non-linear material library for the fibre composite laminate material. Hence, its non-linear constitutive model is discussed in detail. The resulting non-linear constitutive equations for the composite laminate material are coded in FORTRAN as a subroutine and linked to the ABAQUS program.

3.1. Steel reinforcing bar

The reinforcement used in the containment structure is ASTM A-615 Grade 60 steel with yield stress

$$\sigma_y = 413.7 \text{ MPa} \tag{1}$$

and its elastic modulus is assumed to be

$$E_S = 199.9 \text{ GPa} \tag{2}$$

The stress–strain curve of the reinforcing bar is assumed to be elastic–perfectly plastic. In ABAQUS, the steel reinforcement is treated as an equivalent uniaxial material smeared through the element section. In order to properly model the constitutive behaviour of the reinforcement, the cross-sectional area, spacing, position, and orientation of each layer of steel bar within each element need to be specified.

3.2. Steel liner plate and strengthening steel plate

The 0.635 cm liner plate inside the dome and cylinder is ASTM SA-285 Grade A or C carbon steel with yield stress

$$\sigma_y = 165.5 \text{ MPa} \tag{3}$$

The 5.08 cm liner plate on the base slab is ASTM SA-516 Grade 70 stainless steel with yield stress

$$\sigma_y = 262.0 \text{ MPa} \tag{4}$$

In the analysis, the elastic modulus E_S and the Poisson's ratio ν_S of both types of steel liner plates are assumed to be

$$E_S = 199.9 \text{ GPa} \tag{5}$$

$$\nu_S = 0.3 \tag{6}$$

The uniaxial behaviour of the steel liner plate is similar to the reinforcing bar and thus can be simulated by an elastic–perfectly plastic model. When the liner plate is subjected to biaxial stresses, a von Mises yield criterion $f(\sigma_1, \sigma_2)$ is employed to define the elastic limit, where σ_1 and σ_2 are principal stresses and

$$f(\sigma_1, \sigma_2) = \sqrt{\sigma_1^2 + \sigma_1^2 - \sigma_1\sigma_2} = \sigma_y \tag{7}$$

The response of the liner plate is modelled by an elastic–perfectly plastic theory with associated flow rule.

When the containment is strengthened by steel plate at the external surface, it is assumed that the strengthening steel plate has the same material properties and constitutive law as the liner plate inside the dome and cylinder.

3.3. Concrete

The concrete of the containment structure has a uniaxial compressive strength f'_c given as

$$f'_c = 34.47 \text{ MPa} \tag{8}$$

Under uniaxial compression, the concrete strain ε_0 corresponding to the peak stress f'_c is usually around the range of 0.002–0.003. A representative value suggested by ACI Committee 318 [24] and used in the analysis is

$$\varepsilon_0 = 0.003 \tag{9}$$

The Poisson's ratio ν_c of concrete under uniaxial compressive stress ranges from about 0.15 to 0.22, with a representative value of 0.19 or 0.20 [4]. In this study, the Poisson's ratio of concrete is assumed to be

$$\nu_c = 0.2 \tag{10}$$

The uniaxial tensile strength f'_t of concrete is difficult to measure and is normally taken as approximately [4]

$$f'_t = 0.33\sqrt{f'_c} \text{ MPa} \tag{11}$$

The initial modulus of elasticity of concrete E_c is highly correlated to its compressive strength and can be calculated with reasonable accuracy from the empirical equation [24]

$$E_c = 4700\sqrt{f'_c} \text{ MPa} \tag{12}$$

Under different combinations of loading, the failure strengths of concrete are different from that under uniaxial condition. However, the maximum strength enveloped under multiple stress conditions seems to be largely independent of load path [25]. In ABAQUS, a Mohr–Coulomb type compression surface combined with a crack detection surface are used to model the failure surface of concrete (Fig. 3). When the principal stress components of concrete are predominantly compressive, the response of the concrete is modelled by an elastic–plastic theory with associated flow and isotropic hardening rule. In tension, once cracking is defined to occur (by the crack detection surface), the orientation of the crack is stored, and oriented. Damaged elasticity is then used to model the existing crack [23].

When plastic deformation occurs, there should be a certain parameter to guide the expansion of the yield surface. A commonly used approach is to relate the multi-dimensional stress and strain conditions to a pair of quantities, namely, the effective stress σ_c and effective strain ε_c, such that results obtained following different loading paths can all be correlated by means of the equivalent uniaxial stress–strain curve. The stress–strain relationship proposed by Saenz [26] has been widely adopted as the uniaxial stress–strain curve for concrete and it has the following

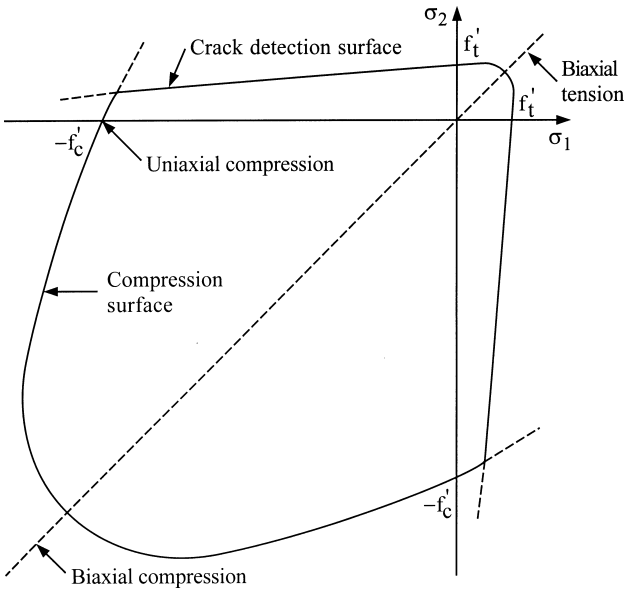

Fig. 3. Concrete failure surface in plane stress.

form

$$\sigma_c = \frac{E_c \varepsilon_c}{1 + (R + R_E - 2)\left(\frac{\varepsilon_c}{\varepsilon_0}\right) - (2R - 1)\left(\frac{\varepsilon_c}{\varepsilon_0}\right)^2 + R\left(\frac{\varepsilon_c}{\varepsilon_0}\right)^3} \tag{13}$$

where

$$R = \frac{R_E(R_\sigma - 1)}{(R_\varepsilon - 1)^2} - \frac{1}{R_\varepsilon}, \qquad R_E = \frac{E_c}{E_0}, \qquad E_0 = \frac{f'_c}{\varepsilon_0}$$

and $R_\sigma = 4$, $R_\varepsilon = 4$ may be used [8]. In the analysis, Eq. (13) is taken as the equivalent uniaxial stress–strain curve for concrete and approximated by several piecewise linear segments as shown in Fig. 4.

When cracking of concrete takes place, a smeared model is used to represent the discontinuous macrocrack behaviour. It is known that the cracked concrete of a reinforced concrete element can still carry some tensile stress in the direction normal to the crack, which is termed as tension stiffening [4]. In this study, a simple descending line is used

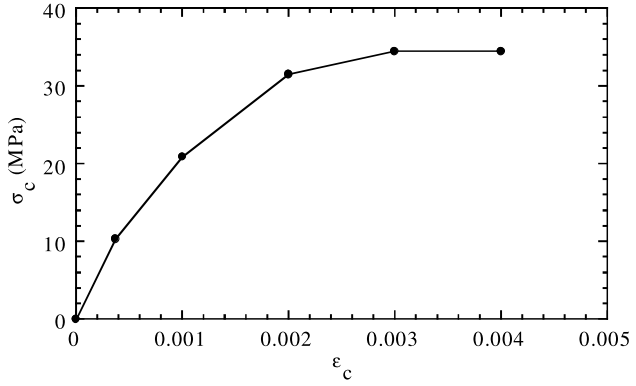

Fig. 4. Equivalent uniaxial stress–strain curve for concrete.

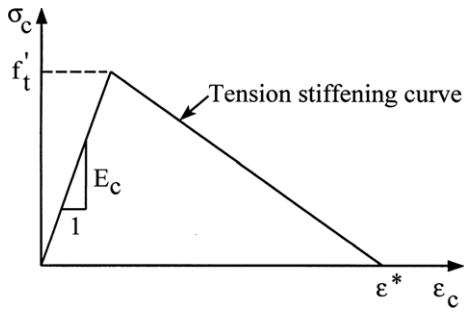

Fig. 5. Tension stiffening model.

to model this tension stiffening phenomenon (Fig. 5). The default value of the strain ε^* at which the tension stiffening stress reduces to zero is [23]

$$\varepsilon^* = 0.001 \tag{14}$$

During the postcracking stage, the cracked reinforced concrete can still transfer shear forces through aggregate interlock or shear friction, which is termed as shear retention. Assuming that the shear modulus of intact concrete is G_c, then the reduced shear modulus G of cracked concrete can be expressed as

$$G = \mu G_c \tag{15}$$

$$\mu = (1 - \varepsilon/\varepsilon_{\max}) \tag{16}$$

where ε is the strain normal to the crack direction and $\varepsilon_{\max}$ is the strain at which the parameter μ reduces to zero. In ABAQUS, $\varepsilon_{\max}$ is usually assumed to be a very large value, i.e. $\mu = 1$ (full shear retention). In this investigation, other than specified, the default values for tension stiffening parameter $\varepsilon^* = 0.001$ and shear retention parameter $\mu = 1$ are used.

3.4. Fibre composite laminate material

For fibre composite laminate materials (Fig. 6), each lamina can be considered as an orthotropic layer in a plane stress condition. The stress–strain relations of the material in fibre and transverse directions, i.e. 1 and 2 directions, are fairly linear. However, severe non-linearity in the in-plane shear stress–strain relation is observed [27]. To model the non-linear in-plane shear behaviour, the non-linear strain–stress relation for a composite lamina suggested by Hahn and Tsai [27] is adopted in this study, which is given as follows:

$$\begin{Bmatrix} \varepsilon_1 \\ \varepsilon_2 \\ \gamma_{12} \end{Bmatrix} = \begin{bmatrix} \frac{1}{E_{11}} & -\frac{\nu_{21}}{E_{22}} & 0 \\ -\frac{\nu_{12}}{E_{11}} & \frac{1}{E_{22}} & 0 \\ 0 & 0 & \frac{1}{G_{12}} \end{bmatrix} \begin{Bmatrix} \sigma_1 \\ \sigma_2 \\ \tau_{12} \end{Bmatrix} + S_{6666}\tau_{12}^2 \begin{Bmatrix} 0 \\ 0 \\ \tau_{12} \end{Bmatrix} \tag{17}$$

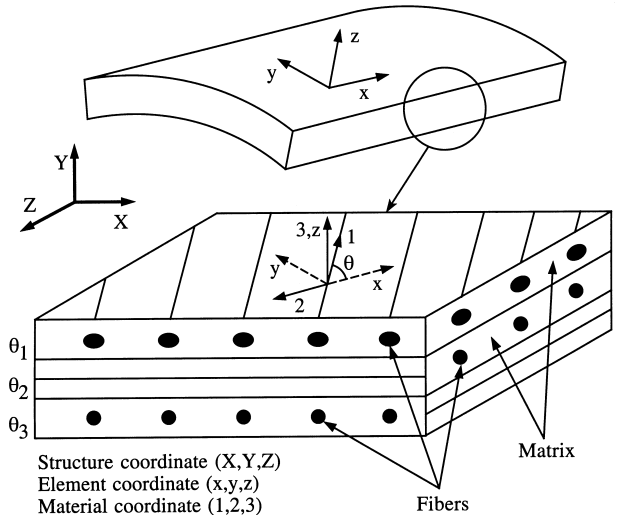

Fig. 6. Material, element and structure coordinates of fibre composite laminate materials.

In this model only one constant S_{6666} is required to account for the in-plane shear non-linearity. The value of S_{6666} can be determined by a curve fit to various off-axis tension test data [27]. Let us define $\Delta\{\sigma'\} = \Delta\{\sigma_1, \sigma_2, \tau_{12}\}^{\mathrm{T}}$ and $\Delta\{\varepsilon'\} = \Delta\{\varepsilon_1, \varepsilon_2, \gamma_{12}\}^{\mathrm{T}}$. Inverting and differentiating Eq. (17), we obtain the incremental stress–strain relations as follows

$$\Delta\{\sigma'\} = [Q_1']\Delta\{\varepsilon'\} \tag{18}$$

$$[Q_1'] = \begin{bmatrix} \dfrac{E_{11}}{1-\nu_{12}\nu_{21}} & \dfrac{\nu_{12}E_{22}}{1-\nu_{12}\nu_{21}} & 0 \\ \dfrac{\nu_{21}E_{11}}{1-\nu_{12}\nu_{21}} & \dfrac{E_{22}}{1-\nu_{12}\nu_{21}} & 0 \\ 0 & 0 & \dfrac{1}{1/G_{12} + 3S_{6666}\tau_{12}^2} \end{bmatrix} \tag{19}$$

Furthermore, it is assumed that the transverse shear stresses always behave linearly and do not affect the non-linear behaviour of in-plane shear. If we define $\Delta\{\tau_t'\} = \Delta\{\tau_{13}, \tau_{23}\}^{\mathrm{T}}$ and $\Delta\{\gamma_t'\} = \Delta\{\gamma_{13}, \gamma_{23}\}^{\mathrm{T}}$, the constitutive equations for transverse shear stresses become

$$\Delta\{\tau_t'\} = [Q_2']\Delta\{\gamma_t'\} \tag{20}$$

$$[Q_2'] = \begin{bmatrix} \alpha_1 G_{13} & 0 \\ 0 & \alpha_2 G_{23} \end{bmatrix} \tag{21}$$

where α_1 and α_2 are the shear correction factors and are taken to be 0.83 in this study.

Among existing failure criteria, the Tsai–Wu criterion [28] has been extensively used and is adopted in this analysis. Under plane stress conditions, this failure criterion has the following form

$$F_1\sigma_1 + F_2\sigma_2 + F_{11}\sigma_1^2 + 2F_{12}\sigma_1\sigma_2 + F_{22}\sigma_2^2 + F_{66}\tau_{12}^2 = 1 \tag{22}$$

and

$$F_1 = \frac{1}{\bar{X}} + \frac{1}{\bar{X}'}, \qquad F_2 = \frac{1}{\bar{Y}} + \frac{1}{\bar{Y}'}, \qquad F_{11} = \frac{-1}{\bar{X}\bar{X}'},$$

$$F_{22} = \frac{-1}{\bar{Y}\bar{Y}'}, \qquad F_{66} = \frac{1}{\bar{S}^2}$$

The $\bar{X}$, $\bar{Y}$ and $\bar{X}'$, $\bar{Y}'$ are the lamina longitudinal and transverse strengths in tension and compression, respectively, and $\bar{S}$ is the shear strength of the lamina. Though the stress interaction term F_{12} in Eq. (22) is difficult to determine, it has been suggested by Narayanaswami and Adelman [29] that F_{12} can be set equal to zero for practical engineering applications. Therefore, $F_{12} = 0$ is used in this investigation.

During the numerical calculation, incremental loading applied to composite plates until failure in one or more individual plies is indicated according to Eq. (22). Since the Tsai–Wu criterion does not distinguish failure modes, the following two rules are used to determine whether the ply failure is caused by resin fracture or fibre breakage [30]:

1. If a ply fails but the stress in the fibre direction remains less than the uniaxial strength of the lamina in the fibre direction, i.e. $\bar{X}' < \sigma_1 < \bar{X}$, the ply failure is assumed to be resin induced. Consequently, the laminate loses its capability to support transverse and shear stresses, but remains to carry longitudinal stress. In this case, the constitutive matrix of the lamina becomes

$$[Q_1'] = \begin{bmatrix} E_{11} & 0 & 0 \\ 0 & 0 & 0 \\ 0 & 0 & 0 \end{bmatrix} \tag{23}$$

2. If a ply fails with σ_1 exceeding the uniaxial strength of the lamina, the ply failure is caused by fibre breakage and total ply rupture is assumed. In this case, the constitutive matrix of the lamina becomes

$$[Q_1'] = \begin{bmatrix} 0 & 0 & 0 \\ 0 & 0 & 0 \\ 0 & 0 & 0 \end{bmatrix} \tag{24}$$

The material properties for fibre composite laminate material used in the analysis are $E_{11} = 128$ GPa, $E_{22} = 11.0$ GPa, $G_{12} = G_{13} = 4.48$ GPa, $G_{23} = 1.53$ GPa, $S_{6666} = 7.31\ (\mathrm{GPa})^{-3}$, $\bar{X} = 1450$ MPa, $\bar{X}' = -1450$ MPa, $\bar{Y} = 52$ MPa, $\bar{Y}' = -206$ MPa, $\bar{S} = 93$ MPa, $\nu_{12} = 0.25$.

During a finite element analysis, the constitutive matrix of composite materials at the integration points of shell elements must be calculated before the stiffness matrices

are assembled from the element level to the structural level. For composite materials, the incremental constitutive equations of a lamina in the element coordinates (x, y, z) can be written as

$$\Delta\{\sigma\} = [Q_1]\Delta\{\varepsilon\} \tag{25}$$

$$\Delta\{\tau_t\} = [Q_2]\Delta\{\gamma_t\} \tag{26}$$

where $\Delta\{\sigma\} = \Delta\{\sigma_x, \sigma_y, \tau_{xy}\}^T$, $\Delta\{\tau_t\} = \Delta\{\tau_{xz}, \tau_{yz}\}^T$, $\Delta\{\varepsilon\} = \Delta\{\varepsilon_x, \varepsilon_y, \gamma_{xy}\}^T$, $\Delta\{\gamma_t\} = \Delta\{\gamma_{xz}, \gamma_{yz}\}^T$, and

$$[Q_1] = [T_1]^T[Q_1'][T_1] \tag{27}$$

$$[Q_2] = [T_2]^T[Q_2'][T_2] \tag{28}$$

$$[T_1] = \begin{bmatrix} \cos^2\theta & \sin^2\theta & \sin\theta\cos\theta \\ \sin^2\theta & \cos^2\theta & -\sin\theta\cos\theta \\ -2\sin\theta\cos\theta & 2\sin\theta\cos\theta & \cos^2\theta - \sin^2\theta \end{bmatrix} \tag{29}$$

$$[T_2] = \begin{bmatrix} \cos\theta & \sin\theta \\ -\sin\theta & \cos\theta \end{bmatrix} \tag{30}$$

The angle θ is measured counter-clockwise from the element local x-axis to the material 1-axis (Fig. 6). Assume $\Delta\{\varepsilon_0\} = \Delta\{\varepsilon_{x0}, \varepsilon_{y0}, \gamma_{xy0}\}^T$ are the incremental in-plane strains at the mid-surface of the shell section and $\Delta\{\kappa\} = \Delta\{\kappa_x, \kappa_y, \kappa_{xy}\}^T$ are the incremental curvatures. The incremental in-plane strains at a distance z from the mid-surface of the shell section become

$$\Delta\{\varepsilon\} = \Delta\{\varepsilon_0\} + z\Delta\{\kappa\} \tag{31}$$

Let h be the total thickness of the composite shell section. The incremental stress resultants, $\Delta\{N\} = \Delta\{N_x, N_y, N_{xy}\}^T$, $\Delta\{M\} = \Delta\{M_x, M_y, M_{xy}\}^T$ and $\Delta\{V\} = \Delta\{V_x, V_y\}$, can be defined as

$$\begin{Bmatrix} \Delta\{N\} \\ \Delta\{M\} \\ \Delta\{V\} \end{Bmatrix} = \int_{-h/2}^{h/2} \begin{Bmatrix} \Delta\{\sigma\} \\ z\Delta\{\sigma\} \\ \Delta\{\tau_t\} \end{Bmatrix} dz \tag{32}$$

Substituting Eqs. (25), (26) and (31) in Eq. (32), leads to the stiffness matrix for the fibre composite laminate shell at the integration point as

$$\begin{Bmatrix} \Delta\{N\} \\ \Delta\{M\} \\ \Delta\{V\} \end{Bmatrix} = \int_{-h/2}^{h/2} \begin{bmatrix} [Q_1] & z[Q_1] & [0] \\ z[Q_1] & z^2[Q_1] & [0] \\ [0]^T & [0]^T & [Q_2] \end{bmatrix} \begin{Bmatrix} \Delta\{\varepsilon_0\} \\ \Delta\{\kappa\} \\ \Delta\{\gamma_t\} \end{Bmatrix} dz \tag{33}$$

where [0] is a 3×2 matrix with all coefficients equal to zero.

4. Numerical analysis

4.1. Ultimate analysis of reinforced concrete containment without strengthening materials

A preliminary ultimate analysis carried out before any fibre composite laminate materials or steel plates are used to strengthen the reinforced concrete containment [13]. The containment is subjected to an internal pressure and a dead load due to its own weight. It is assumed that the dead load, w_c, caused by the reinforced concrete [31] is

$$w_c = 23.56 \text{ kN m}^{-3} \tag{34}$$

Fig. 7 shows the internal pressure p versus the displacement of node 1 (at the apex of the containment) in the z-direction. Due to the dead load, the apex of the containment has an initial downward (negative) displacement at the beginning of the analysis. When the internal pressure is increased, the apex of the containment gradually moves upward up to failure. When the containment is about to fail, there is a significant ductile deformation at the apex. The ultimate internal pressure p_u of the containment is 164.6 kPa which is about 59.2% higher than the design pressure capacity 103.4 kPa [14]. The deformation shape of the containment under the ultimate internal pressure is shown in Fig. 8a and the crack patterns of the concrete at the inner and outer sides of the containment are shown in Fig. 8b. From these figures, it can be seen that under the ultimate pressure, the base slab remains in contact with the ground. Most of the deformation takes place in the upper cylinder and dome. In addition, due to stress concentration, cracks are likely to occur near the apex of the dome, the conjunction of dome and cylinder, and the mid-cylinder location where the thickness changes abruptly.

4.2. Ultimate analysis of reinforced concrete containment strengthened by composite materials or steel plates at the upper cylinder

From the preliminary study it is observed that the upper portion of cylinder has significant deformation under the

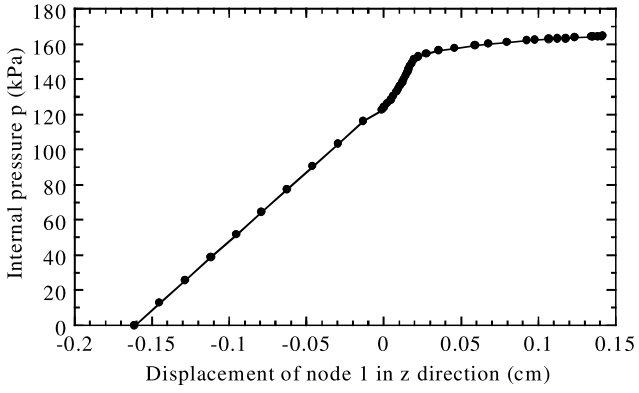

Fig. 7. Load–displacement curve of reinforced concrete containment without strengthening materials.

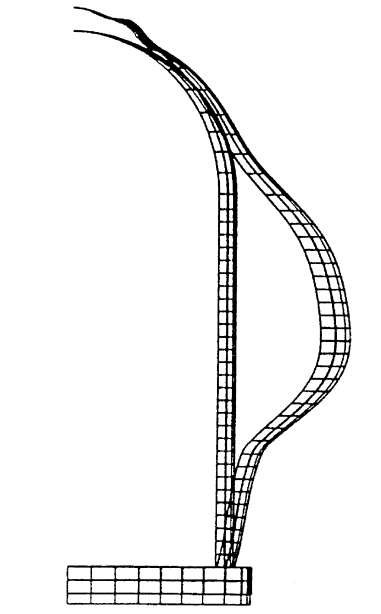

(a) Deformation shape

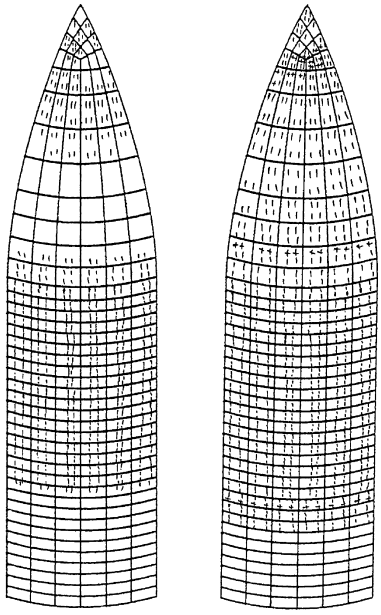

(b) Crack patterns

Fig. 8. Deformation shape and crack patterns for reinforced concrete containment under the ultimate load (without strengthening materials).

ultimate load. This is because the thickness as well as the stiffness of the upper cylinder is significantly less than those of the low cylinder. Hence, numerical studies of the containment strengthened by a composite material at the entire upper cylinder, whose thickness is 1.067 m, are carried out. The laminate lay-ups for the composite materials are $[90/0]_{10S}$, $[\pm 45/90/0]_{5S}$ and $[\pm\theta/90/0]_{5S}$. The thickness of each lamina is 4 mm and the total thickness of the entire

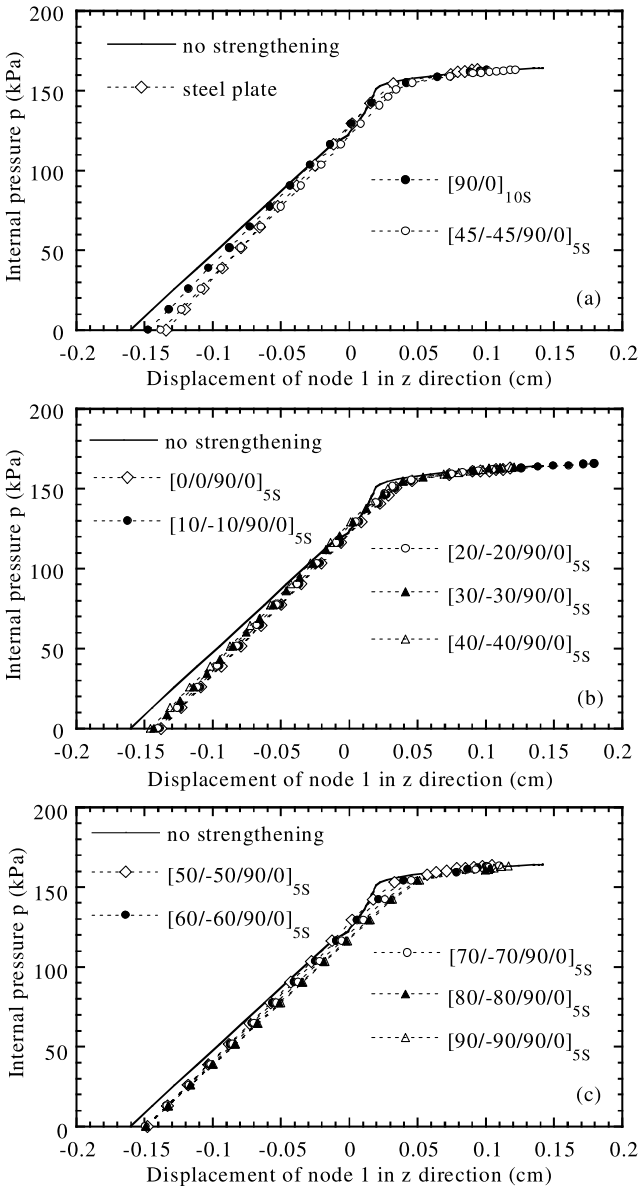

Fig. 9. Load–displacement curves of reinforced concrete containment strengthened by steel plates and composite laminate materials at the upper cylinder.

cross-section of the composite material is 16 cm. The fibre angle of the lamina is measured counter-clockwise (through the outward normal direction) from the meridian of the containment shell structure. Hence, 0 and 90° would be in the meridian direction and the hoop direction of the shell, respectively. For comparison, numerical studies of the containment strengthened by steel plate at the entire upper cylinder are also performed. The thickness of the strengthening steel plate is assumed to be 10 cm.

Fig. 9 shows the internal pressure p versus the displacement of node 1 in the z-direction for the containment strengthened by steel plate or various types of composite laminate lay-ups. All the curves show similar trends to that without the use of any strengthening and none of them could

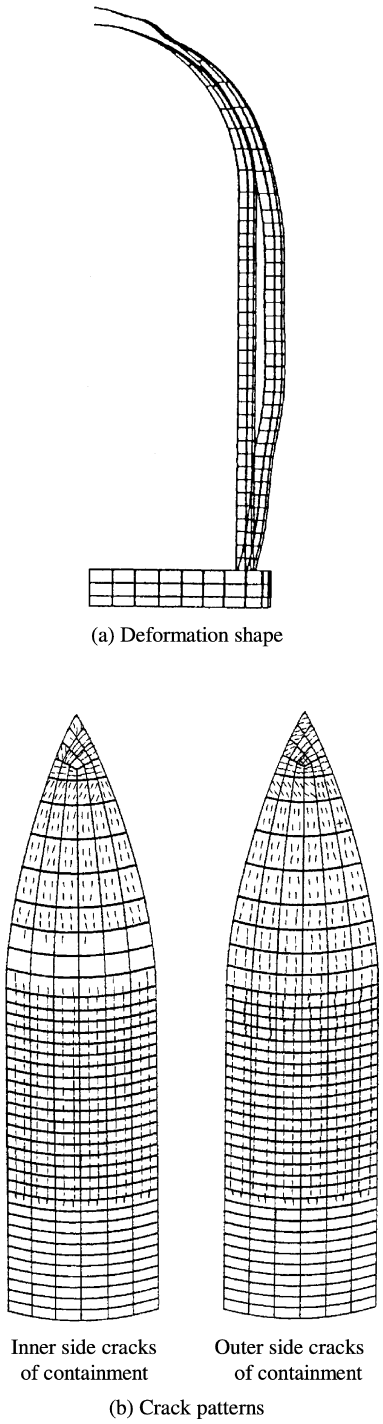

Fig. 10. Deformation shape and crack patterns for reinforced concrete containment under the ultimate load (strengthened with $[\pm 45/90/0]_{5S}$ composite material at the upper cylinder).

increase the stiffness as well as the ultimate strength of the containment. Fig. 10 shows typical deformation and crack patterns of the containment strengthened by composite materials with $[\pm 45/90/0]_{5S}$ lay-up under the ultimate load stage. Although the deformation of the containment at the upper cylinder (Fig. 10a) is smaller than that without the use of strengthening materials (Fig. 8a), more extensive cracks take place near the apex of the strengthened containment than that of the unstrengthened one. Once the apex fails, the containment cannot resist further loads. Hence, it may be concluded that the apex of the dome is the weakest point of the containment structure and the use of strengthening steel plates or composite materials with any types of lay-ups at the upper cylinder will be in vain.

4.3. Ultimate analysis of reinforced concrete containment strengthened by composite materials or steel plates at the dome

Based on the results of Section 4.2, numerical studies of the containment strengthened by composite materials or steel plates at the entire hemispherical dome are carried out. The laminate lay-ups for the composite materials are the same as before: $[90/0]_{10S}$, $[\pm 45/90/0]_{5S}$ and $[\pm\theta/90/0]_{5S}$. The thicknesses of the composite lamina and steel plate are also the same as before.

Fig. 11 shows the internal pressure p versus the displacement of node 1 in the z-direction for containments strengthened by steel plate or various types of composite laminate lay-ups. Fig. 11a shows that the behaviour of the containment strengthened by the $[\pm 45/90/0]_{5S}$ composite material is similar to that strengthened by the steel plate. While the containment strengthened by the $[90/0]_{10S}$ composite material has a lower stiffness than the former pair, all the strengthened containments have significantly higher ultimate strengths than the unstrengthened one. However, these strengthened containments all fail in brittle patterns and no noticeable ductile deformation occurred at the apex. The behaviours of the containments strengthened by the $[\pm\theta/90/0]_{5S}$ composite materials at the dome can generally be separated into two groups. When $0 \leq \theta \leq 40°$, the use of composite materials increases the stiffness as well as the ultimate strength of the containment (Fig. 11b). When $50 \leq \theta \leq 90°$, using composite materials does not increase the stiffness of the containment but only improves the ultimate strength of the containment (Fig. 11c). Nevertheless, all containments strengthened by the $[\pm\theta/90/0]_{5S}$ composite materials also fail in brittle patterns.

Fig. 12 shows the typical deformation and crack patterns of the containment strengthened by composite materials with $[\pm 45/90/0]_{5S}$ lay-up under the ultimate load stage. It can be observed that by strengthening the dome, the upper cylinder of the containment undergoes more deformation (Fig. 12a) than that without the use of strengthening materials (Fig. 8a). Although the strengthened dome has much less cracks (Fig. 12b) than the unstrengthened one (Fig. 8b), extensive cracks still take place at the junction of the dome and cylinder and the mid-cylinder location where the thickness changes abruptly. Hence, it may be concluded that after the dome is strengthened, the upper cylinder becomes the weakest part of the containment.

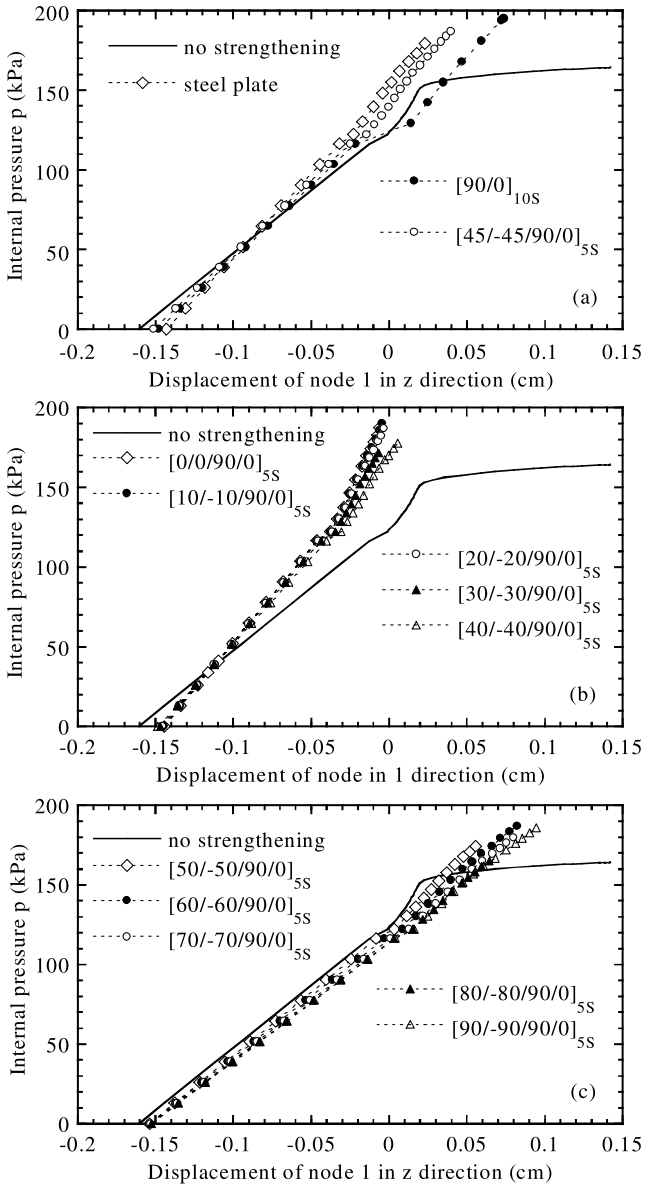

Fig. 11. Load–displacement curves of reinforced concrete containment strengthened by steel plates and composite laminate materials at the dome.

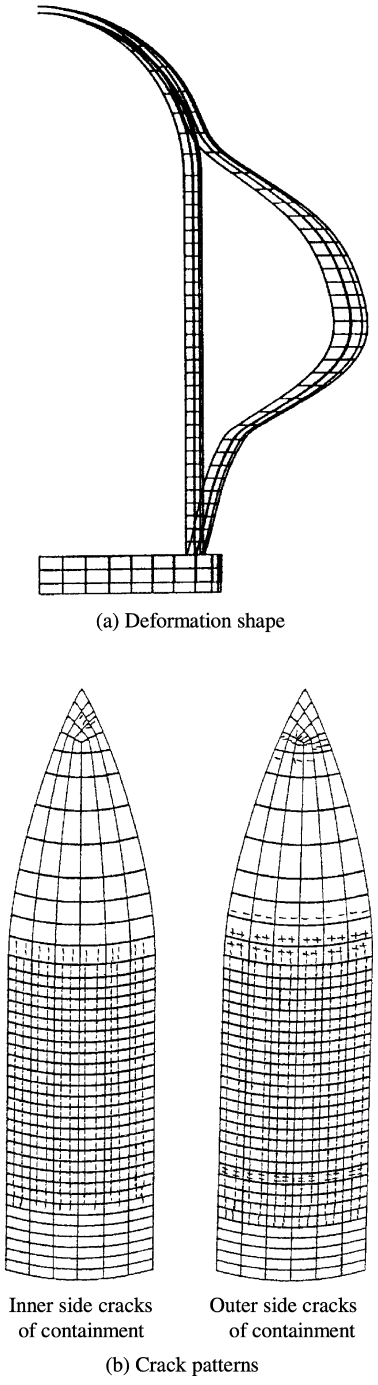

Fig. 12. Deformation shape and crack patterns for reinforced concrete containment under the ultimate load (strengthened with $[\pm 45/90/0]_{5S}$ composite material at the dome).

4.4. Ultimate analysis of reinforced concrete containment strengthened by composite materials or steel plates at the upper cylinder and dome

Based on the results of Section 4.3, numerical studies of the containment strengthened by composite materials or steel plates at both the upper cylinder and dome are carried out. The laminate lay-ups and thickness for the composite materials are the same as before. The thickness of the strengthening steel plate is reduced to 5 cm.

Fig. 13 shows the internal pressure p versus the displacement of node 1 in the z-direction for containments strengthened by steel plate or various types of composite laminate lay-ups. Fig. 13a is similar to Fig. 12a. It shows that the behaviour of the containment strengthened by the $[\pm 45/90/0]_{5S}$ composite material is similar to that strengthened by the steel plate whereas the containment strengthened by the $[90/0]_{10S}$ composite material has lower stiffness. Although the three strengthened containments have significantly higher ultimate strengths than the unstrengthened one, they all fail in brittle patterns and no noticeable ductile deformation occurred at the apex. The behaviours of the containments strengthened by the $[\pm\theta/90/0]_{5S}$ composite

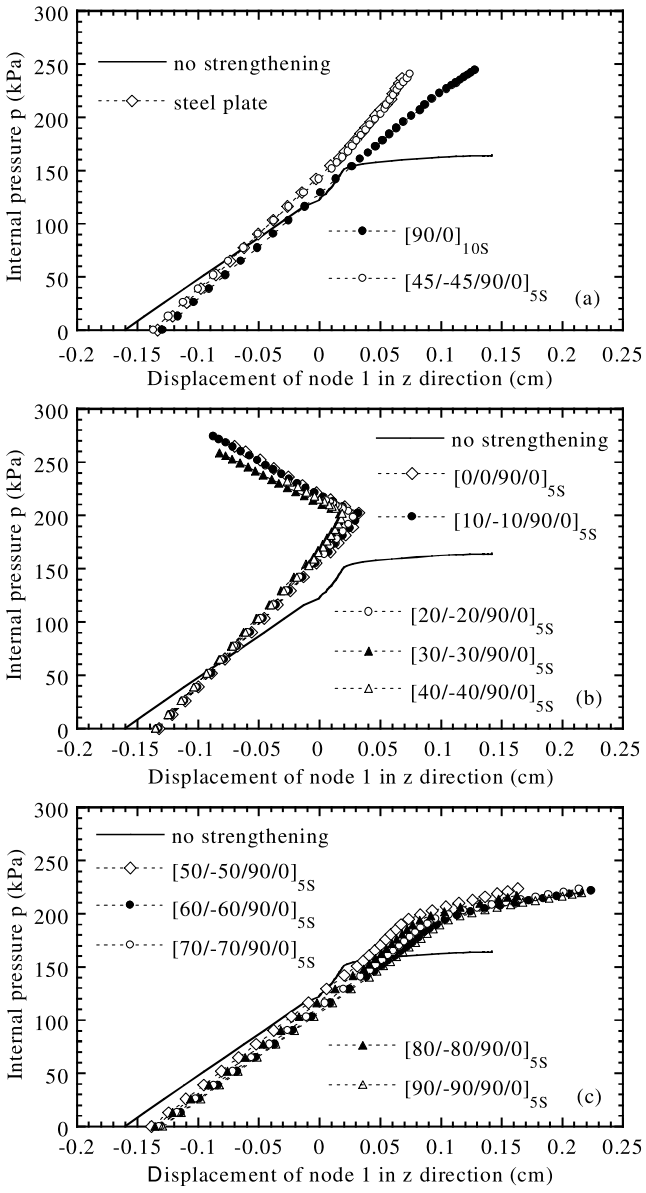

Fig. 13. Load–displacement curves of reinforced concrete containment strengthened by steel plates and composite laminate materials at the upper cylinder and dome.

materials at the upper cylinder and dome again can be separated into two groups. For $0 \leq \theta \leq 40°$, the containments exhibit hardening behaviour before the structures fail (Fig. 13b). For $50 \leq \theta \leq 90°$, the containments exhibit softening behaviour (Fig. 13c) and significant ductile deformation takes place at the apex when the containments are about to fail. Nevertheless, all containments strengthened by the $[\pm\theta/90/0]_{5S}$ composite materials have much higher ultimate strengths than the unstrengthened one. For example, the ultimate strength of the containment strengthened by the $[\pm 50/90/0]_{5S}$ composite materials is 223.7 kPa, which is higher than the unstrengthened value 164.6 kPa by 35.9% and higher than the design pressure capacity 103.4 kPa by 116.3%.

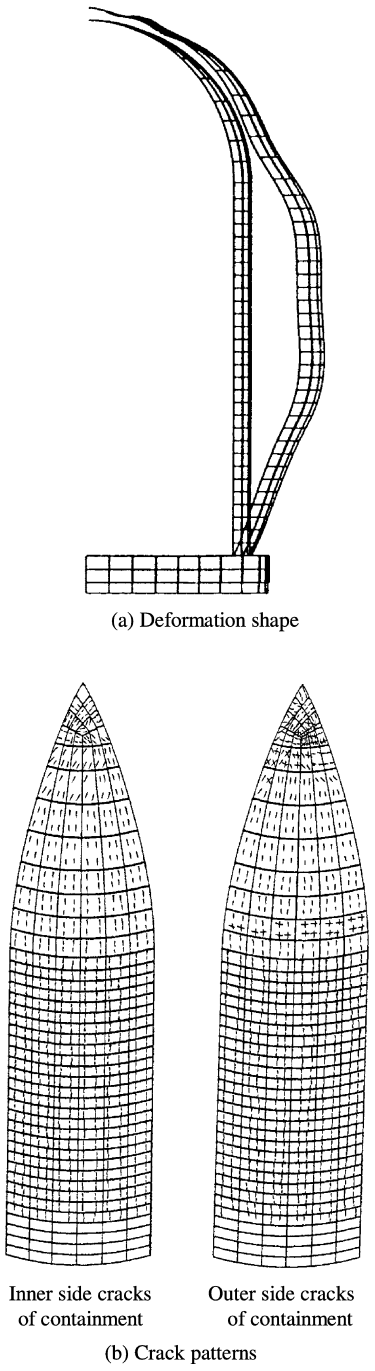

Fig. 14. Deformation shape and crack patterns for reinforced concrete containment under the ultimate load (strengthened with $[\pm 45/90/0]_{5S}$ composite material at the upper cylinder and dome).

Fig. 14 shows the typical deformation and crack patterns of the containment strengthened by composite materials with $[\pm 45/90/0]_{5S}$ lay-up under the ultimate load stage. It can be observed that by strengthening the upper cylinder and dome, the entire containment undergoes more uniform and smooth deformation (Fig. 14a) than that without the use of strengthening materials (Fig. 8a). When the containment fails, severe cracks exist near the apex of the dome and the

junction of the dome and cylinder. It seems that the apex of the dome and the junction of the dome and cylinder are about to fail at the same time. Due to the concerns of ductile behaviour and high ultimate strength, it is suggested to employ the $[\pm\theta/90/0]_{5S}$ composite materials with $50 \leq \theta \leq 90^\circ$ to strengthen the reinforced concrete containment at the upper cylinder and the dome simultaneously.

5. Conclusions

In this paper, non-linear finite element analyses of the BWR Mark III reinforced concrete containment at Kuosheng nuclear power plant strengthened by composite materials or steel plates are performed. For simplicity, equipment hatches and penetrations on the containment are not considered. Based on the numerical results, the following conclusions may be drawn:

1. The apex of the dome is the weakest point of the containment structure and the use of strengthening steel plates or composite materials with any types of lay-ups at the upper cylinder will be in vain.
2. The use of steel plates or composite materials with $[90/0]_{10S}$ or $[\pm 45/90/0]_{5S}$ lay-ups to strengthen the containment at the dome only or at both the upper cylinder and the dome simultaneously, generally gives higher ultimate strengths than the unstrengthened one. However, due to their brittle failure patterns, the use of steel plates or composite materials with $[90/0]_{10S}$ or $[\pm 45/90/0]_{5S}$ lay-ups to strengthen the containment is not suggested.
3. The use of composite materials with $[\pm\theta/90/0]_{5S}$ lay-ups to strengthen the containment at the dome also renders higher ultimate strengths and brittle failure patterns and is not suggested.
4. The use of $[\pm\theta/90/0]_{5S}$ composite materials with $0 \leq \theta \leq 40^\circ$ to strengthen the containment at the upper cylinder and dome yields hardening behaviour to the containment and this may not be desired.
5. The use of $[\pm\theta/90/0]_{5S}$ composite materials with $50 \leq \theta \leq 90^\circ$ to strengthen the containment at the upper cylinder and dome leads to softening behaviour and ductile deformation to the containment. In addition, the ultimate strengths of these strengthened containments are much higher than the unstrengthened one. Thus, the use of $[\pm\theta/90/0]_{5S}$ composite materials with $50 \leq \theta \leq 90^\circ$ to strengthen the reinforced concrete containment at the upper cylinder and the dome simultaneously is recommended.

Acknowledgements

This research work was financially supported by the Taiwan Power Company via the National Science Council, Republic of China under Grant NSC 89-TPC-7-006-016.

References

[1] US Nuclear Regulatory Commission, Office of Nuclear Reactor Regulation. Standard review plan for the review of safety analysis reports for nuclear plants, section 3.8.1, NUREG-0800. 1987.
[2] Amin M, Eberhardt AC, Erler BA. Design considerations for concrete containments under severe accident loads. Nucl Engng Des 1993;145:331–8.
[3] Boeck BD. A review of containment accidents. Nucl Engng Des 1993;145:279–88.
[4] ASCE Task Committee on Concrete and Masonry Structure. State of the art report on finite element analysis of reinforced concrete. New York: ASCE, 1982.
[5] Chen WF. Plasticity in reinforced concrete. New York: McGraw-Hill, 1982.
[6] Meyer C, Okamura H. Finite element analysis of reinforced concrete structures. New York: ASCE, 1985.
[7] Vecchio FJ, Collins MP. The modified compression-field theory for reinforced concrete elements subjected to shear. ACI J 1986;83:219–31.
[8] Hu H-T, Schnobrich WC. Nonlinear finite element analysis of reinforced concrete plates and shells under monotonic loading. Comput Struct 1991;38:637–51.
[9] Borri A, Sorace S. FE analysis strategies for structural materials with small tensile strength. J Pres Ves Technol 1993;115:156–63.
[10] Pfeiffer PA, Kennedy JM, Marchertas AH. Post-test analysis for the nonlinear response of an internally pressurized one sixth scale reinforced concrete containment model. Nucl Engng Des 1992;133:143–57.
[11] Andreoli V, Angeloni P, Contri P, Brusa L. Numerical simulation of the ultimate capacity of a reactor containment building. Nucl Engng Des 1993;145:403–17.
[12] Saito H, Muramatsu Y, Furukawa H, Hasegawa T, Mutoh A. Post-test analysis of a 1:10-scale top slab model of ABWR/RCCV subjected to internal pressure. Nucl Engng Des 1993;145:339–53.
[13] Hu H-T, Liang J-I. Ultimate analysis of BWR Mark III reinforced concrete containment subjected to internal pressure. Nucl Engng Des 2000;195(1):1–11.
[14] Taiwan Power Company, Final Safety Analysis Report. Kuosheng Nuclear Power Station Units 1 and 2, vol. 5. 1979.
[15] Baker AA. Fibre composite repair of cracked metallic aircraft components—practical and basic aspects. Composite 1987;18(4):293–308.
[16] Ong CL, Chu RC, Ko TC, Shen SB. Composite patch reinforcement of cracked aircraft upper longeron: analysis and specimen simulation. Theor Appl Fract Mech 1990;14:13–26.
[17] Naboulsi S, Mall S. Modeling of a cracked metallic structure with bonded composite patch using the three layer technique. Compos Struct 1996;35:295–308.
[18] Schubbe JJ, Mall S. Investigation of a cracked thick aluminum panel repaired with a bonded composite patch. Engng Fract Mech 1999;63:305–23.
[19] Ritchie PA, Thomas DA, Lu L-W, Connelly GM. External reinforcement of concrete beams using fibre reinforced plastics. ACI Struct J 1991;88(4):490–500.
[20] Nanni A. Flexural behaviour and design of RC members using FRP reinforcement. J Struct Engng (ASCE) 1993;119(11):3344–59.
[21] Sharif A, Al-Sulaimani GJ, Basunbul IA, Baluch MH, Ghaleb BN. Strengthening of initially loaded reinforced concrete beams using FRP plates. ACI Struct J 1994;91(2):160–7.
[22] GangaRao HVS, Vijay PV. Bending behaviour of concrete beams wrapped with carbon fabric. J Struct Engng (ASCE) 1998;124:3–10.

[23] Hibbitt, Karlsson & Sorensen, Inc. ABAQUS theory manual and user manual, Version 5.8. Providence, Rhode Island, 2000.
[24] ACI Committee 318. Building code requirements for structural concrete and commentary (ACI 318-99). Detroit, Michigan: American Concrete Institute, 1999.
[25] Kupfer H, Hilsdorf HK, Rusch H. Behaviour of concrete under biaxial stresses. ACI J 1969;66:656–66.
[26] Saenz LP. Discussion of equation for the stress–strain curve of concrete by Desayi P, Krishnan S. ACI J 1964;61:1229–35.
[27] Hahn HT, Tsai SW. Nonlinear elastic behaviour of unidirectional composite laminae. J Compos Mater 1973;7:102–18.
[28] Tsai SW, Wu EM. A general theory of strength for anisotropic materials. J Compos Mater 1971;5:58–80.
[29] Narayanaswami R, Adelman HM. Evaluation of the tensor polynomial and Hoffman strength theories for composite materials. J Compos Mater 1977;11:366–77.
[30] Rowlands RE. Strength (failure) theories and their experimental correlation. In: Sih GC, Skudra AM, editors. Failure mechanics of composites. The Netherlands: Elsevier, 1985. p. 71–125.
[31] Wang C-K, Salmon CG. Reinforced concrete design. 6th ed. New York: Addison-Wesley, 1998. Chapter 1.